01 Jan 2023

High-Temperature Interactions Between Titanium Alloys And Strontium Zirconate Refractories

R. Sharon Uwanyuze
Missouri University of Science and Technology, ruvhg@mst.edu

Baris Yavas

Jiyao Zhang

Janos E. Kanyo

et. al. For a complete list of authors, see https://scholarsmine.mst.edu/matsci_eng_facwork/3251

Recommended Citation

R. S. Uwanyuze et al., "High-Temperature Interactions Between Titanium Alloys And Strontium Zirconate Refractories," *Journal of Materials Engineering and Performance*, Springer; ASM International, Jan 2023. The definitive version is available at https://doi.org/10.1007/s11665-023-08597-8

JMEPEG
https://doi.org/10.1007/s11665-023-08597-8

1059-9495/$19.00

ORIGINAL RESEARCH ARTICLE

High-Temperature Interactions Between Titanium Alloys and Strontium Zirconate Refractories

R. Sharon Uwanyuze, Baris Yavas, Jiyao Zhang, Janos E. Kanyo, Lesley D. Frame, Rainer J. Hebert, Stefan Schafföner, and S. Pamir Alpay

Submitted: 23 April 2023 / Revised: 17 July 2023 / Accepted: 30 July 2023

We investigated interactions between Ti6Al4V alloys and strontium zirconate ($SrZrO_3$) ceramic to assess its potential as a refractory mold material in investment casting. We developed a robust yet simple procedure to examine both the liquid–solid and solid–solid interactions using pellets in drop casting and diffusion couple methods. Reaction layers were characterized using optical microscopy, scanning electron microscopy (SEM), transmission electron microscopy (TEM), and x-ray diffraction (XRD). The results were compared to alumina (Al_2O_3) which is still a common refractory ceramic for molds in investment casting. Our findings indicate that Ti6Al4V surfaces in contact with $SrZrO_3$ had no apparent changes in surface chemistry nor microstructure. On the other hand, Ti6Al4V surfaces in contact with Al_2O_3 developed γ-TiAl and α_2-Ti_3Al intermetallics with thicknesses of $\sim$ 100 μm in diffusion couples and $\sim$ 10 μm in drop-casting experiments. Nanoindentation results showed that the surface of Ti6Al4V in contact with Al_2O_3 was significantly harder compared to $SrZrO_3$, confirming our conclusion. Given the time and costs associated with mechanical and chemical removal of reaction layers on Ti6Al4V castings, $SrZrO_3$ can be a better choice for a mold material in the investment casting of titanium alloys.

Keywords investment casting, refractories, strontium zirconate, Ti6Al4V, titanium

1. Introduction

Titanium alloys are highly versatile materials, valued for their light weight, high-temperature strength, corrosion resistance, fracture toughness, and biocompatibility. As a result, they are used in a wide range of applications, including aerospace, biomedical, marine, and chemical industries (Ref 1-4). Among titanium alloys, Ti6Al4V is often considered the workhorse of titanium metallurgy, making up over half of the total volume of titanium used in airframe parts (Ref 5-7). This is due to the alloy's exceptional mechanical properties, which stem from its alpha and beta phase (α+β) microstructure, enabling high impact and fatigue strength, ductility, and fracture toughness.

Manufacturing titanium alloys efficiently can be challenging, however, due to their high melting temperatures and the high affinity of titanium for interstitial impurities such as oxygen, nitrogen, and carbon. This affinity issue often results in the formation of an alpha case layer on the surface that is harder and more brittle than the bulk material (Ref 8-11). In a series of computational studies, we investigated how surfaces of titanium and titanium alloys, including those containing aluminum and vanadium, interact with interstitial elements such as oxygen, hydrogen, and nitrogen, as well as some substitutional elements (Ref 12-14). It is now understood that, in addition to interstitial elements, the alpha case can also contain increased amounts of substitutional elements, such as aluminum dissolved from the mold (Ref 11, 15). This layer must be removed through secondary processing to maintain uniform properties and microstructure (Ref 16-18). However, such additional steps increase manufacturing time and cost, thereby hindering near-net shape production.

Investment casting is a well-established manufacturing method for producing precise and complex titanium alloy parts, with high productivity and minimal metal scrap wastage compared to machining (Ref 19, 20). The process starts with repeatedly coating a wax pattern with layers of refractory ceramic slurry and stucco until a desired thickness. The assembly is then dried and placed in an autoclave oven to melt the wax leaving a hollow shell mold (Ref 21). The mold is sintered at high temperatures of over 1000 °C to increase its strength. Molten metal is then poured into the shell molds to form desired castings.

To produce parts with a good surface finish, it is necessary to prevent metal-mold reactions. Characteristics of an ideal mold material for titanium metallurgy include a high melting temperature to withstand titanium melts of about 1700 °C with superheat, creep and oxidation resistance, and chemical inertness in highly reducing atmospheres. Significant efforts have gone into finding suitable mold materials to prevent the persistent problem of metal-mold reactions (Ref 8, 10, 22, 23). Refractory ceramics for metallurgical applications must withstand thermomechanical stresses and high-temperature metal-

Distribution A. Approved for public release: distribution unlimited (AFRL-2023-1200); date approved 03-10-2023.

R. Sharon Uwanyuze, Baris Yavas, Jiyao Zhang, Janos E. Kanyo, Lesley D. Frame, Rainer J. Hebert, and **S. Pamir Alpay**, Department of Materials Science and Engineering and Institute of Materials Science, University of Connecticut, Storrs; **Stefan Schafföner**, Department of Ceramic Materials Engineering, University of Bayreuth, Bayreuth, Germany. Contact e-mail: pamir.alpay@uconn.edu.

Published online: 10 August 2023

mold interactions that often lead to surface contamination of the alloy. Such reactions also impair the knock-out removal process of the metal parts from the ceramic molds, and can alter the alloy surface properties like ductility, fracture toughness and fatigue life (Ref 11, 24, 25). As such, there is a need to find more inert refractories for titanium metallurgy. Alumina is still a common refractory (Ref 26-28), although yttria, zirconia and calcia have been explored as well (Ref 29-32). Al_2O_3 has high strength and is abundantly available and cheap. Nonetheless, there are studies that have reported reactions between Al_2O_3 and titanium alloys during melting and casting (Ref 33-35). Therefore, there is a need for a fuller understanding of the reactions observed experimentally to design more corrosion-resistant molds.

Novel alkaline earth zirconate materials such as calcium zirconate ($CaZrO_3$), barium zirconate ($BaZrO_3$) and strontium zirconate ($SrZrO_3$) are very promising refractories that have the combination of properties required for titanium metallurgy (Ref 35-39). For instance, the melting temperatures of $SrZrO_3$, $CaZrO_3$, and $BaZrO_3$ are approximately 2800 °C, 2368 °C, and 2700 °C, respectively (Ref 40). Additionally, these materials have a perovskite structure which is highly close-packed (Ref 41, 42). $SrZrO_3$, in particular, has been noted for its high corrosion resistance especially in alkaline melts and vapors (Ref 43). Nonetheless, even though $SrZrO_3$ has been studied as a thermal barrier coating and an electrical insulator (Ref 44-46), there is very little research that has explored it as a mold material for titanium alloy casting.

The objective of this study is to evaluate $SrZrO_3$ as a viable mold material for Ti6Al4V alloy in investment casting. Two methods were devised to investigate the formation of reaction products between $SrZrO_3$ and Ti6Al4V at elevated temperatures, simulating the pouring and solidification steps of the investment casting process by drop casting and diffusion couples, respectively. The performance of $SrZrO_3$ is compared to Al_2O_3 under the same conditions, and recommendations are given based on detailed characterization and hardness test data.

2. Methods

Ti6Al4V (grade 5 titanium, McMaster Carr, USA) was used as the metallic substrate. It was received with the expected $\alpha+\beta$ microstructure as displayed in Fig. 1. Powders and then pellets of $SrZrO_3$ were successfully produced in-house through solid state synthesis between high-purity $SrCO_3$ (Seaforth Mineral & Ore, USA) and ZrO_2 (Imerys Fused Minerals, USA) (Ref 47). Alumina powders (CTC40, Almatis, USA) were similarly pressed and sintered into sample pellets according to the proceeding procedure. Figure 2 illustrates the two main methods applied to investigate the high-temperature chemical stability of the refractory ceramics in contact with Ti6Al4V.

$SrZrO_3$ samples were produced through calcination of $SrCO_3$ and ZrO_2, then pressed, and sintered. During the first step, CO_2 evaporates, and the remaining strontium oxide reacts with zirconia to form $SrZrO_3$ via the following reactions:

$$SrCO_3 \rightarrow SrO + CO_2 (900\ ^\circ C) \quad \text{(Eq 1)}$$

$$SrO + ZrO_2 \rightarrow SrZrO_3 (1200\ ^\circ C) \quad \text{(Eq 2)}$$

Calcination was performed in a conventional air atmosphere furnace (HT 40/17, Nabertherm, Germany) with a target temperature of 1200 °C held for 6 h. A 1-2-h hold at 900 °C was introduced to ensure full decomposition of $SrCO_3$ to SrO. The calcined blocks were then ground and milled to $< 63\ \mu m$ $SrZrO_3$ powders. Both $SrZrO_3$ and Al_2O_3 powders were divided into 2 and 5 g batches for pressing 12 and 20 mm diameter pellets, respectively. A 5 wt.% polyvinyl alcohol (PVA) solution was used as a binder. The binder solution was pipetted into each batch in a ratio of one drop per gram of powder, and thoroughly mixed until there were no more agglomerates. The mixture was then pressed to 20 MPa in a lubricated die (WD-40, Grainger, USA) for smooth demolding. The pellets were sintered to 1650 °C with a maximum temperature dwell time of 6 hours and stepwise heating rates explained in our previous work (Ref 47).

Diffusion couple experiments were performed to investigate solid-solid interface reactions between the Ti-alloy and test ceramic at 1350 °C for up to 5 h, to assess potential reactions during solidification of a cast part. The couples consisted of a Ti6Al4V alloy between two ceramic pellets of either Al_2O_3 or $SrZrO_3$ as demonstrated in Fig. 2(a). Before the experiments, all the ceramic and metal samples were polished to a mirror-finish to ensure maximum contact of the diffusion couple interfaces. They were ground with silicon carbide papers of successively increasing grit, #180, #320, and #600, then polished with diamond particle suspensions of 9, 3 and 1 μm (Allied High-Tech Products, USA). The metal samples were finished off with a 0.04 μm colloidal silica polish, and all the samples were thoroughly washed with soap and water then passed through a 2 minute- ultrasonic bath of ethanol. The samples were placed in a drying oven at 60 °C for at least 8

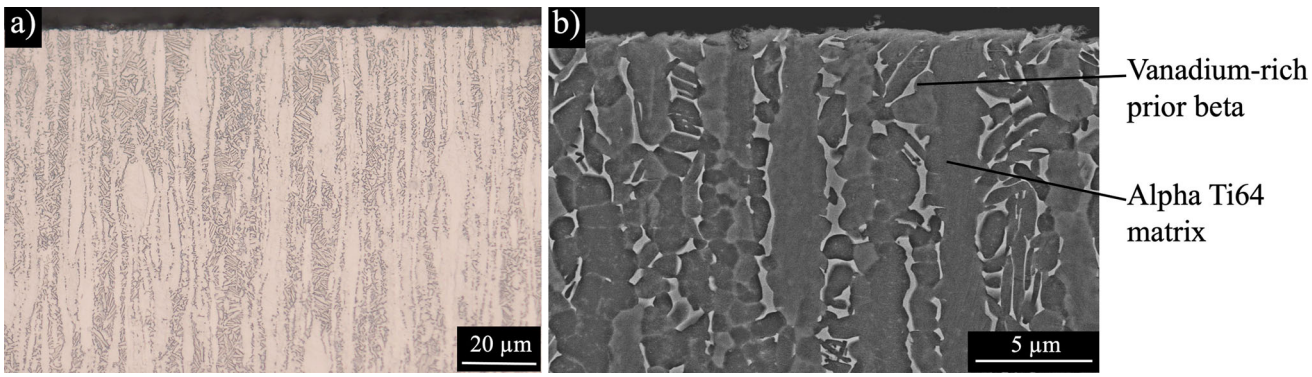

Fig. 1 As received cross-sectional microstructure of Ti6Al4V: (a) Optical microscope (OM), and (b) backscatter electron (BSE) SEM images.

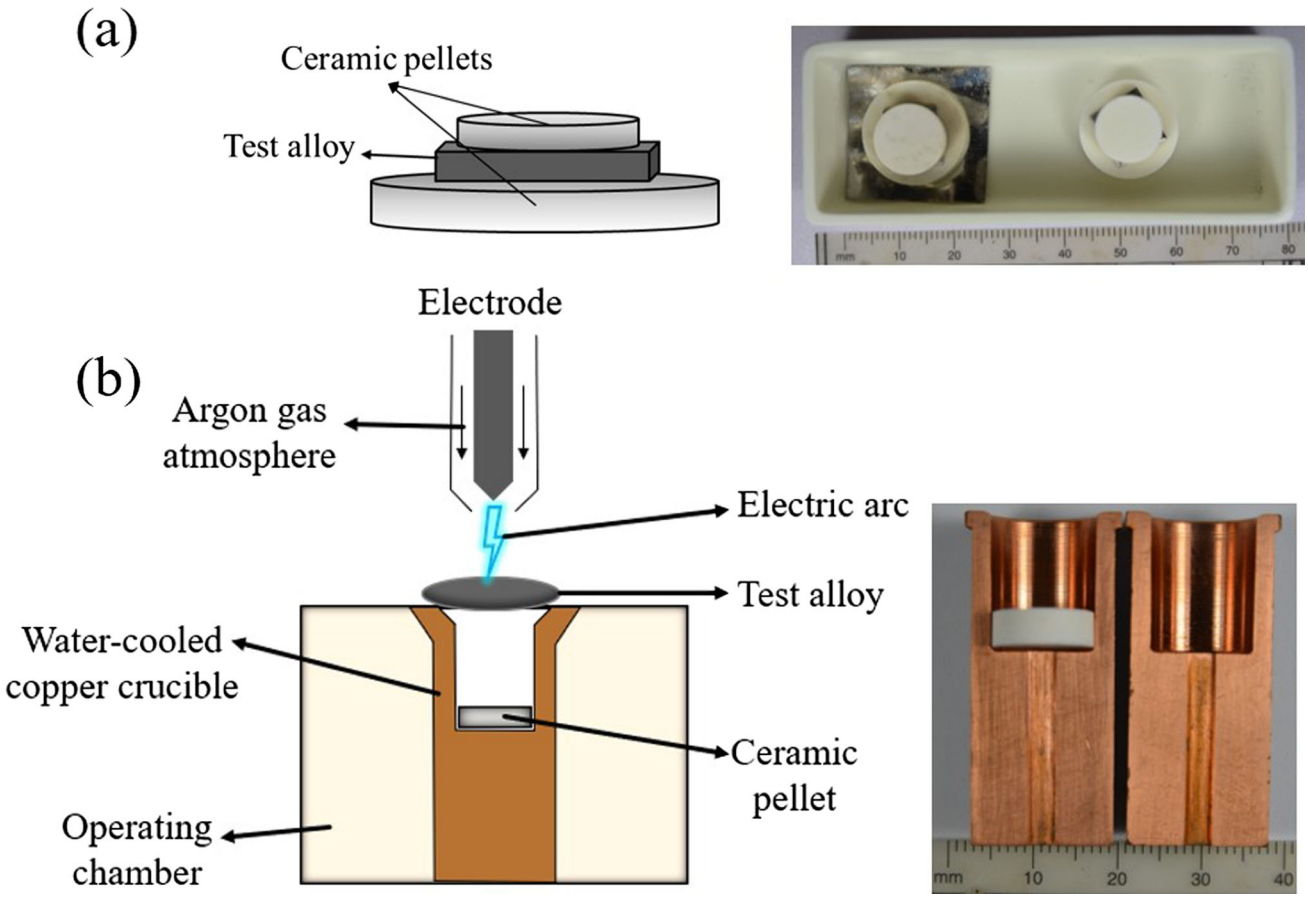

Fig. 2 Methods applied to investigate metal-mold reactions between Ti6Al4V with $SrZrO_3$ versus Al_2O_3, (a) diffusion couples and (b) drop casting

hours to remove moisture. Diffusion couple analysis was performed in a tube furnace (RHTH 50-150/18, Nabertherm, Germany). The samples were placed in an alumina crucible for the experiment, but the $SrZrO_3$ pellets were put on a platinum or MgO substrate and not directly on the crucible to prevent high-temperature reaction with alumina. The arrangement with the bigger pellet at the bottom and the smaller pellet on top ensured good stability when transferring samples in and out of the furnace. The furnace was intermittently purged thrice with high-purity argon gas ($>$99.999%) as vacuum was being drawn. During our experiments, the argon atmosphere was maintained at a flowrate of 200 cc/min. The samples were heated to 1350 °C at 200 °C/h, and held for 5 hours before naturally cooling to room temperature in the furnace.

Drop casting is a method that replicates investment casting on a smaller scale, and it was successfully used in the examination of metal-mold reactions between various ceramics and titanium alloys (Ref 15, 48). We employed drop casting to assess interface interactions of Ti6Al4V with Al_2O_3 and $SrZrO_3$ using an arc melting furnace (MAM 1, Edmund Buhler, Germany). However, our setup was modified to use a ceramic pellet to represent an idealized mold wall, and the pellet was inserted in a customizable water-cooled copper crucible as displayed in Fig. 2(b). The test alloy sample was placed at the mouth of the copper crucible, and when melted by the arc, it dropped directly onto the ceramic in the crucible. The atmosphere in the furnace was controlled in the range of 1×10^{-1} Pa by a rotary pump, and argon was backfilled to the pressure of $\sim 5 \times 10^{3}$ Pa.

An x-ray diffractometer (SmartLab, Rigaku, USA) equipped with a rotating Cu anode source was used to identify reaction phases on post-reaction Ti6Al4V surfaces. The measurement parameters were set to a 2-theta range of 20-95°, step size of 0.02°, and a rate of 5°/min in Bragg Brentano configuration. We also used GIXRD to examine reaction products near sample surface compared to those deeper in the bulk of the Ti6Al4V samples. An ω angle of 1.0° was applied for GIXRD, which scans to about 95 nm depth, assuming at least 63% of the x-ray incident beam contributes to the measured intensity.

For microscopy analysis, the samples were first mounted in epoxy (EpoThin2, Buehler, USA) to ensure any surface reaction layers stayed intact. Sectioning followed using a silicon carbide blade on cutting saw (TechCut 4, Allied High-Tech Products, USA). Lastly, the samples were re-mounted for grinding and polishing to expose the cross section for characterization. The same sequence previously described for the pre-experiment sample preparation was applied. The Ti6Al4V portions were etched using Kroll's reagent for about 5 seconds with the swap method to achieve better contrast images. An optical microscope (Axio Imager A2, Zeiss, USA) was used to investigate a large microstructure area. Next, a detailed reaction layer examination was performed with an SEM equipped with electron-dispersive x-ray spectroscopy (FEI Teneo–ThermoFisher Scientific, USA). The SEM was

operated at an accelerating voltage of 10 kV with 1.6 nA applied on samples that were pre-coated with a 10-nm layer of carbon to minimize charging, especially from the ceramics and epoxy mounts. The specific areas of interest on the rection regions were investigated with a Talos 200 TEM (Thermo-Fisher Scientific, USA). TEM samples were prepared by focused ion beam (FIB) technique.

Mechanical testing was performed on cross-sectioned, mounted, and polished diffusion couple samples using a nanoindenter (iNano, KLA Instruments, USA). A load of 5 mN was selected, and 8 × 8 matrices with a 5 μm distance between rows and columns were defined starting on the Ti6Al4V side, followed by the interface, and then the ceramic bulk material.

3. Evaluation of Metal-Mold Reactions via Diffusion Couples

In the present study, the surface microstructure and properties of the metal samples were compared before and after the experiments. As shown in Fig. 1, the Ti6Al4V sample initially exhibited a uniform microstructure at the surface, where the vanadium-rich β phase extended from bulk to surface. However, high-temperature processing of this alloy in contact with Al_2O_3 resulted in significant diffusion of elemental aluminum from the ceramic into the metal surface, thus, changing the surface microstructure. Figure 3(a) shows a cross section of the Ti6Al4V sample that was in contact with Al_2O_3 during the diffusion couple experiment. The surface changes are clear in both the optical and higher magnification backscatter electron SEM image. As observed in Fig. 3(b), the vanadium-rich β no longer extended from bulk to surface, but instead a higher concentration of aluminum was detected at the alloy surface than in the bulk, which is an α-phase stabilizer (Ref 49). The diffusion-affected zone from the interface into the bulk where the vanadium-rich veins resumed was an average of 75 μm (see labels 1-3). The EDS mapping and point analysis from these three regions display clear variations in the concentration of aluminum. Region 1, which was closest to the Al_2O_3 ceramic showed 46.1 at.% Al, while that in region 2 had 23.9 at.% Al and region 3 had 16.0 at.% Al. The possible phases in these regions were thus inferred to be γ-TiAl in the top layer, α_2-Ti_3Al in the subsurface layer, and α-Ti in the immediate bulk. These reaction products are consistent with the Ti-Al phase diagram (Ref 50). For conservation of mass, O_2 also diffused but to a limited concentration that only formed a solid solution with the titanium alloy and no secondary phase layer. Notably, an α-case comprises of a reaction layer and a diffusion-hardened layer (Ref 9-11). The reaction layer was made up of γ-TiAl and α_2-Ti_3Al, while the hardened layer was mainly α-Ti with dissolved O_2.

The Ti6Al4V sample in contact with $SrZrO_3$ displayed no apparent changes. Figure 4 illustrates that the bulk microstructure of the alloy extends to the surface, and there was no diffusion of strontium or zirconium from the ceramic into the metal surface. Nonetheless, a thin oxide scale of less than 1 μm was detected on the surface by EDS (Fig. 4b). The O_2 is expected to be from $SrZrO_3$, but no cation diffusion of Sr or Zr was observed. Therefore, no intermetallic reaction products formed as was the case on the Ti6Al4V sample in contact with Al_2O_3 (Fig. 3b). The goal is to keep any oxide scale to a minimal thickness with no altering effect on the subsurface microstructure, which was obtained on the alloy sample in contact with $SrZrO_3$.

A comparison of the phases at the surface and deeper into the bulk of the Ti6Al4V samples that were in contact with Al_2O_3 and $SrZrO_3$ is shown in Fig. 5. GIXRD enabled us to profile reaction products at the metal surface up to 95 nm deep, while conventional XRD profiled through a thickness of up to 3.8 μm. The Ti6Al4V sample that was in contact with Al_2O_3 had γ-TiAl and α_2-Ti_3Al within the subsurface, which agreed with the EDS results presented in Fig. 3. Contrarily, there were

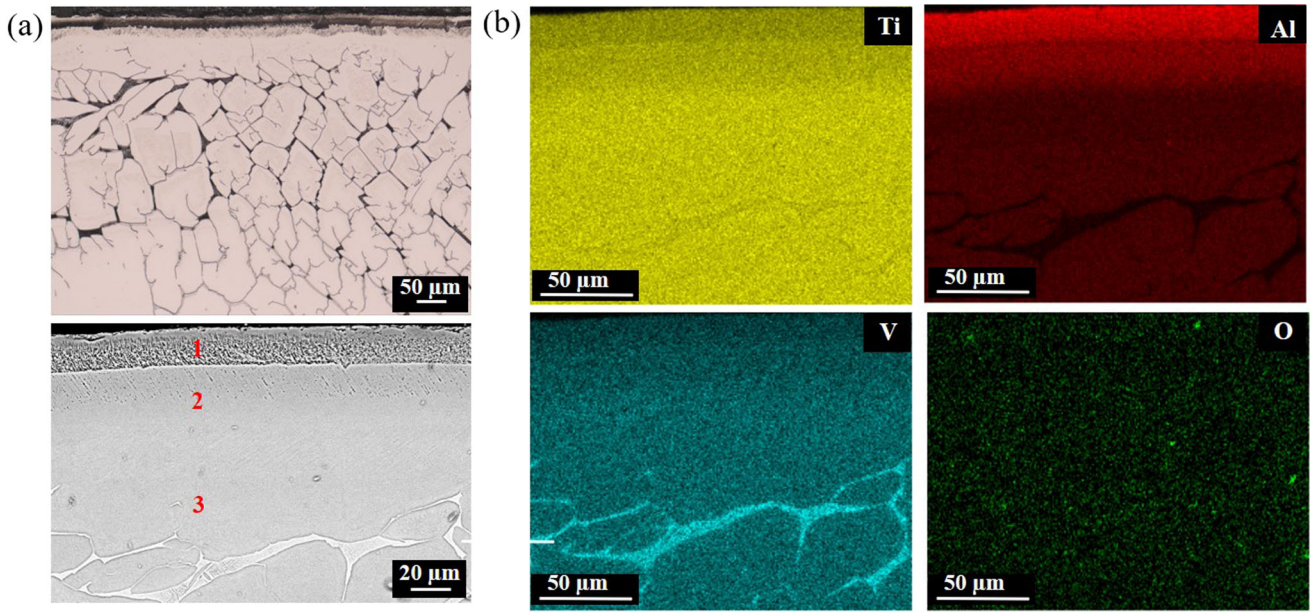

Fig. 3 Ti6Al4V that was in contact with Al_2O_3 during the diffusion couple experiment; (a) wide area OM image in the top and higher magnification BSE SEM images of the cross section in the bottom; (b) the compositional maps were extracted from EDS spectrum image data acquired by scanning repeatedly over the area shown in the BSE SEM image

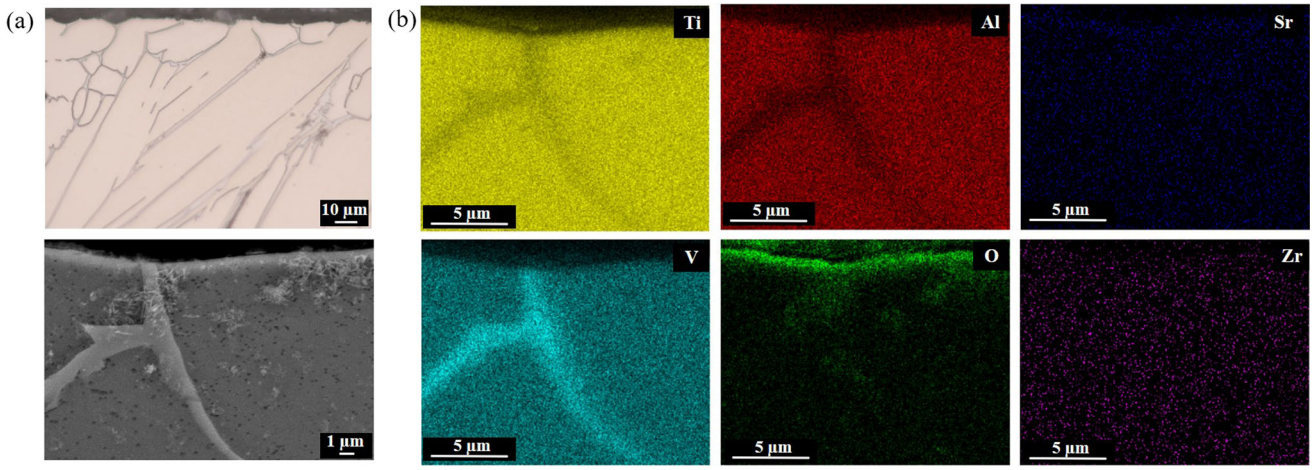

Fig. 4 Ti6Al4V that was in contact with SrZrO3 in the diffusion couple experiments: (a) OM image and higher magnification BSE SEM images of the cross section; (b) the compositional maps from EDS spectrum image data acquired by scanning repeatedly over the area shown in the BSE SEM image

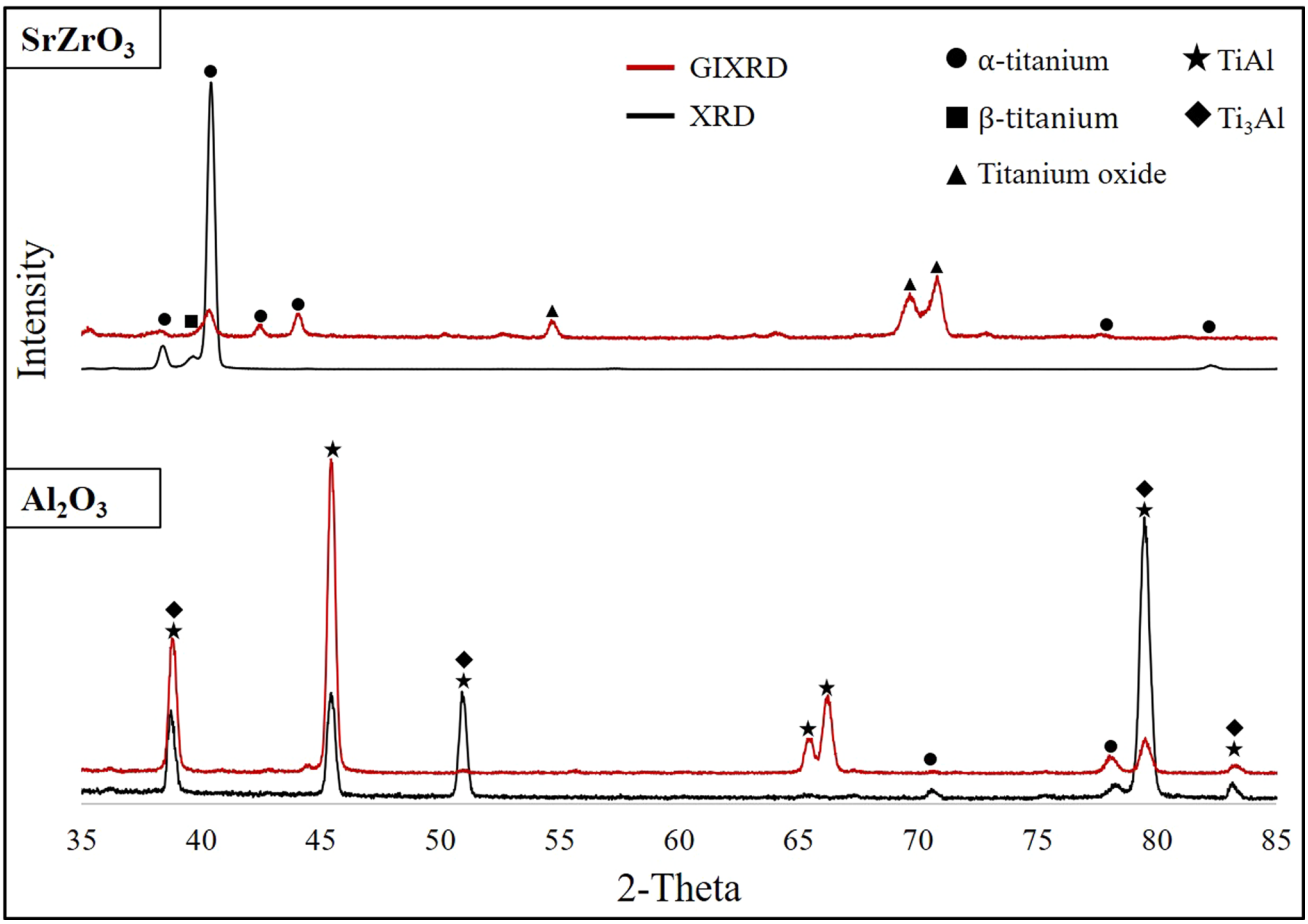

Fig. 5 XRD and GIXRD data obtained from the contact surface of Ti6Al4V. Post-diffusion couples in contact with SrZrO3 and Al_2O_3. PDF file numbers used for phase identification are 03-065-9622 (α-Ti), 01-089-3726 (β-Ti). 01-084-1750 (TiO_2), 00-009-0098 (Ti3Al), 00-005-0678 (TiAl)

no observed intermetallic reaction products with the $SrZrO_3$ ceramic. Therefore, since both sets of samples were exposed to the same parameters and the only difference was the ceramic compositions, we conclude that the increased aluminum was from Al_2O_3, and not segregation from Ti6Al4V nor contamination from the furnace components.

4. Analysis of Metal-Mold Reactions on Drop-Cast Ti6Al4V

The phenomenon in drop casting correlates to the thin metal surface that touches the mold wall during investment casting, while the diffusion couples model the metal interior of the casting as it is cooling over a more extended time period. Interestingly, the trend observed using the diffusion couple method was similar to what we observed in the drop-cast samples (Fig. 6, 7, 8, 9), but much smaller in terms of thicknesses of the interaction layers at the Ti6Al4V surface because of significantly less contact time. Notably, Ti6Al4V cast onto Al_2O_3 had ceramic adhered to the metal after solidification and there was a reaction layer formed between the ceramic and the alloy as shown in Fig. 6. A FIB lift-out from the interface through the Ti6Al4V matrix was taken from the cross section for further investigations using TEM. The EDS maps (Fig. 7) exhibited clear concentration differences, even though there was no defined border in terms of the elemental distributions. The reaction layer and interface were aluminum-rich and titanium-deficient compared to the matrix in the bulk. A set of selected area diffraction patterns (SADPs) were obtained in TEM mode by tilting both the matrix and reaction layer to well-defined zone axes as shown in Fig. 7. The matrix corresponds to the zone axis [01 $\bar{1}$ 0] from α-Ti (HCP a: 2.906 Å, c: 4.667 Å) even at the Al-rich interface, whereas the reaction layer matched with the [0001] zone axis from Ti_3Al (HCP a: 5.764 Å, c: 4.664 Å). The matrix and reaction layer had different microstructures. However, we did not see a γ-TiAl phase on the drop-cast samples like in the diffusion couples. Unlike Ti_3Al, γ-TiAl forms after a higher amount of Al has diffused into the metal. Therefore, since the drop-cast samples solidified rapidly, there was insufficient time for such extended diffusion to occur.

Ti6Al4V cast on $SrZrO_3$ exhibited no observable reaction layer (Fig. 8). A FIB lift-out was still taken from this interface and EDS maps confirmed that there was no strontium nor zirconium diffusion into the alloy as shown in Fig. 9. There was only a very thin nanometer range oxygen-rich layer at the surface, much thinner than in the diffusion couple.

5. Surface Hardness Studies via Nanoindentation

Metal-mold reactions change the surface mechanical properties of cast parts, and a typical method for measuring this impact is through hardness testing (Ref 9-11). Figure 10 shows hardness plots as a function of depth from the Ti6Al4V matrix through the interface to the bulk ceramic. Indentation was performed on the cross section of diffusion couple samples with 64 indents in each of the three regions. As seen in these maps, the hardness in the Ti6Al4V in contact with Al_2O_3, Fig. 10(a), increased gradually from the metal matrix through the reaction layer at the interface. On the other hand, the hardness in the Ti6Al4V sample in contact with $SrZrO_3$, Fig. 10(b), did not change between the matrix and the interface. These observations are quantified in Fig. 10(c) which confirms that the average surface hardness on the two Ti6Al4V samples was different based on the ceramics they interacted.

6. Proposed Mechanism

Figure 11 illustrates the mechanism we propose for the microstructure evolution as reaction products form on Ti6Al4V in contact with Al_2O_3. The initial microstructure of Ti6Al4V is the expected α-phase in the matrix and β-phase at the grain boundaries. At the dwell temperature (1350 °C), elemental aluminum from Al_2O_3 diffuses gradually into the metal surface. Al combines with Ti at the surface leading to formation of α_2-Ti_3Al. With increasing time, the α_2-Ti_3Al layer grows thicker, and a thin top layer of γ-TiAl which has the highest concentration of diffused Al develops closest to the Al_2O_3. When Ti6Al4V is at elevated temperatures, the diffusivity of Al in titanium is higher than that of V [0.105 versus 0.065 $\mu m^2/s$ at 950 °C (Ref 51). Therefore, vanadium remains in the bulk far from the surface as seen in Fig. 3 and 6. Oxygen also diffuses into the alloy, but up to a known solubility limit of about 16 at.% through the α_2-Ti_3Al and 2 at.% through γ-TiAl (Ref 52, 53). Formation of the titanium aluminide reaction products hinders further diffusion of oxygen; thus, no apparent oxide scale can be seen. The phases most attributed to increased

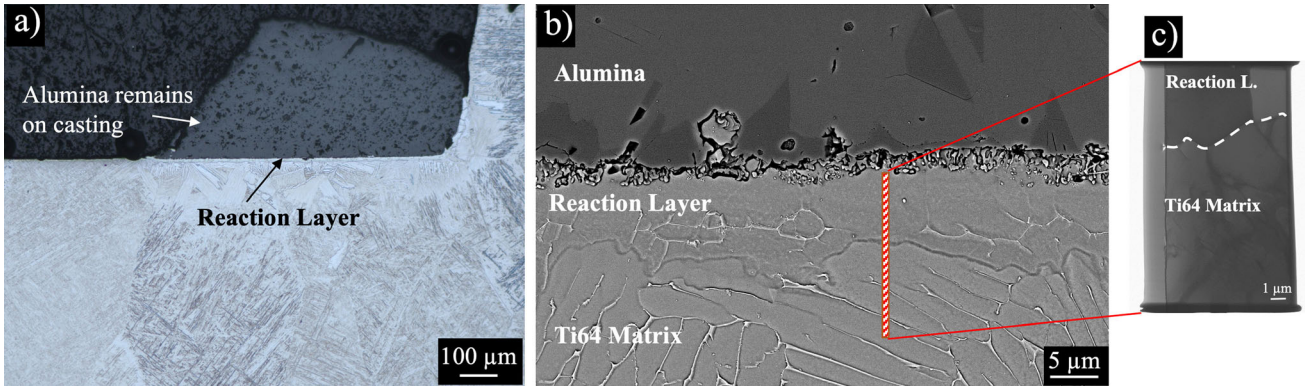

Fig. 6 Drop casting of Ti6Al4V on Al_2O_3. (a) The OM image showed ceramic remains on the casting, and (b) the metal surface underneath these Al_2O_3 remains had an altered microstructure from the bulk. (c) The FIB sample was lifted out from the edge of the cross section for TEM analysis

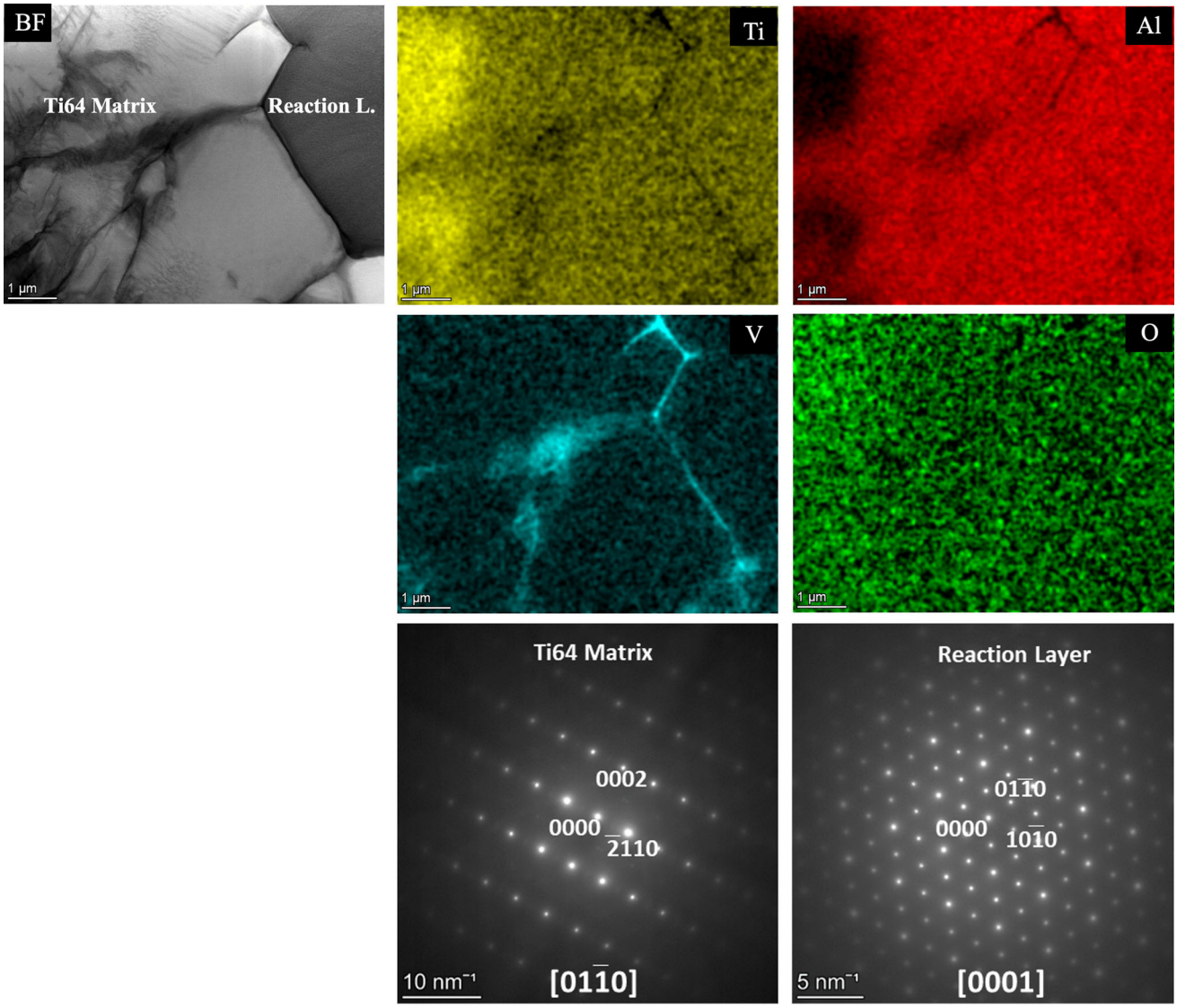

Fig. 7 STEM and TEM data obtained from Ti6Al4V sample drop-cast on Al_2O_3. The EDS compositional maps and SADPs were extracted from the areas shown in the BF image. Phase identification matched α-Ti (HCP a: 2.906 Å, c: 4.667 Å) in the matrix, and Ti_3Al (HCP a: 5.764 Å, c:4.664 Å) in the reaction layer

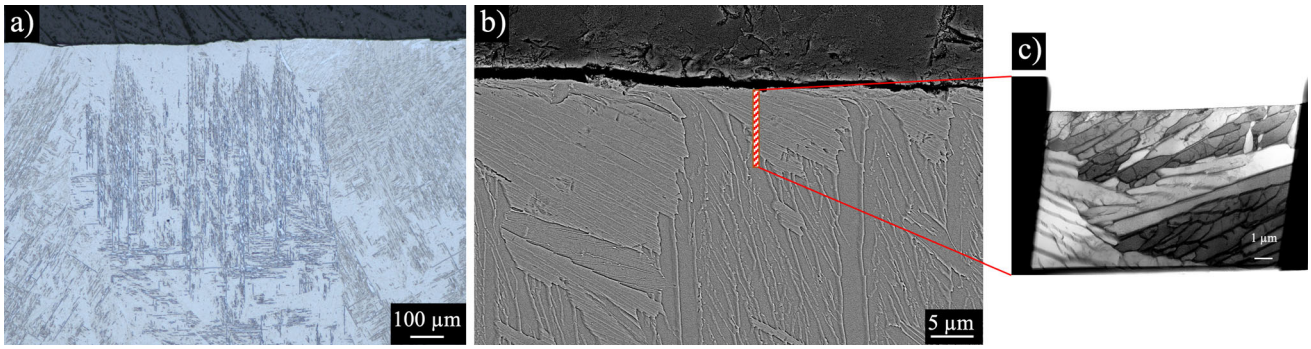

Fig. 8 Drop casting of Ti6Al4V on $SrZrO_3$. There was no observable change in the microstructure as seen from the (a) OM, (b) SEM and (c) TEM images, respectively.

hardness on the Ti6Al4V sample were γ-TiAl and α_2-Ti_3Al. These phases were characterized using XRD and TEM diffraction and their stoichiometry agrees with the Ti-Al phase diagram (Ref 50). Other studies involving diffusion bonding of Ti6Al4V to Al_2O_3 also reported similar phases (Ref 54, 55).

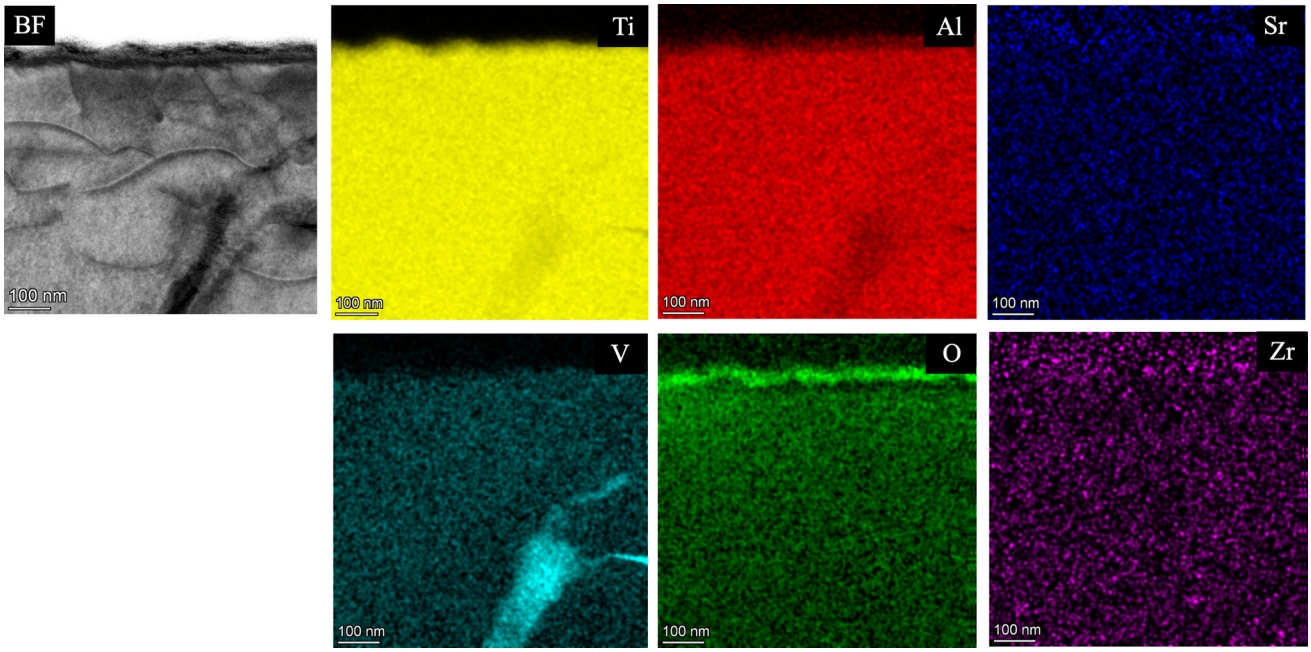

Fig. 9 STEM data obtained from Ti6Al4V drop-casting sample on $SrZrO_3$. The compositional maps were extracted from EDS spectrum image data acquired by scanning repeatedly over the area shown in the BF STEM image.

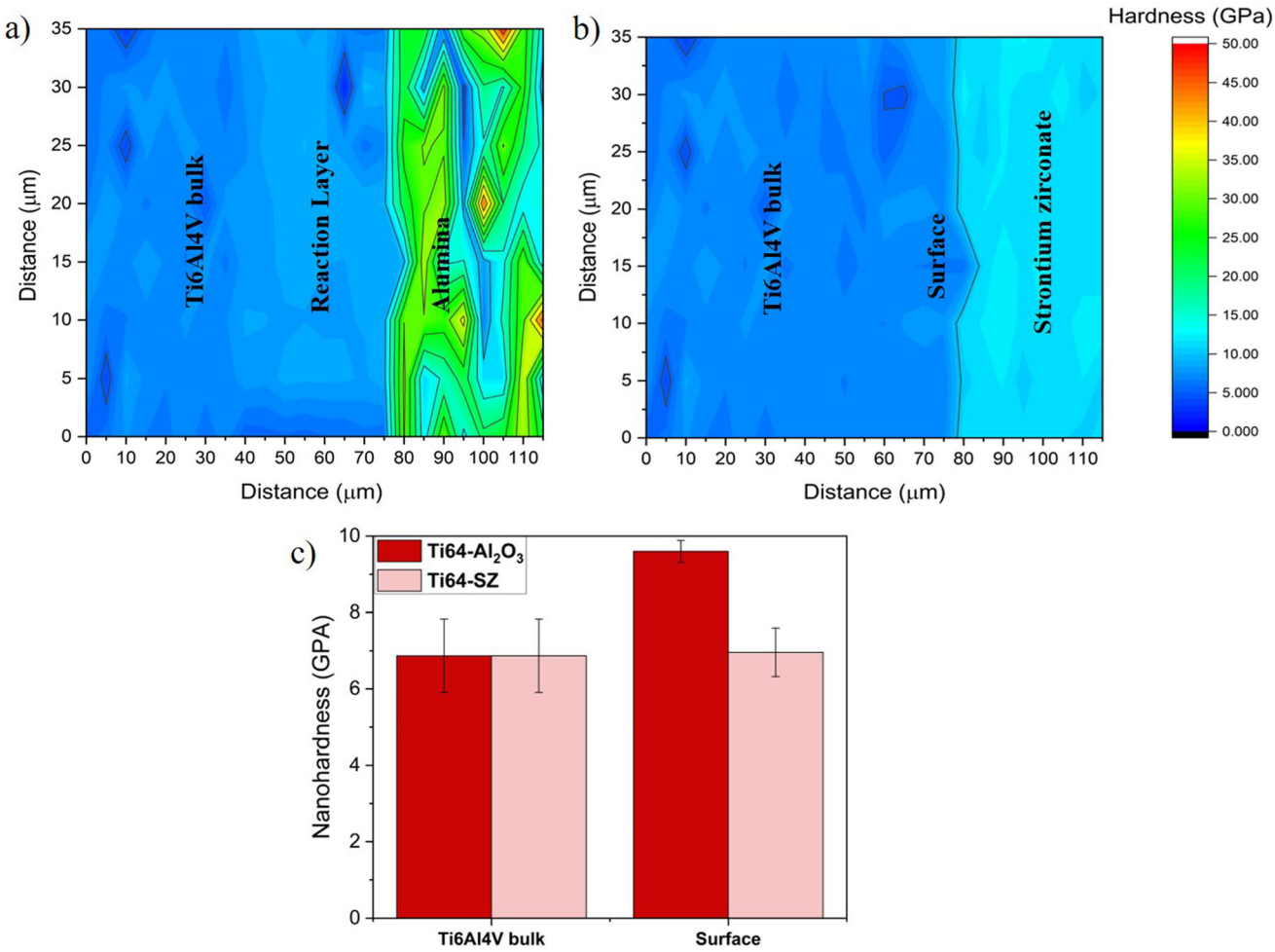

Fig. 10 Nano-hardness differences between the bulk Ti6Al4V and the surfaces in contact with (a) Al_2O_3 and (b) $SrZrO_3$. The bar graph (c) shows the average hardness in each region, and the error bars represent the standard deviation.

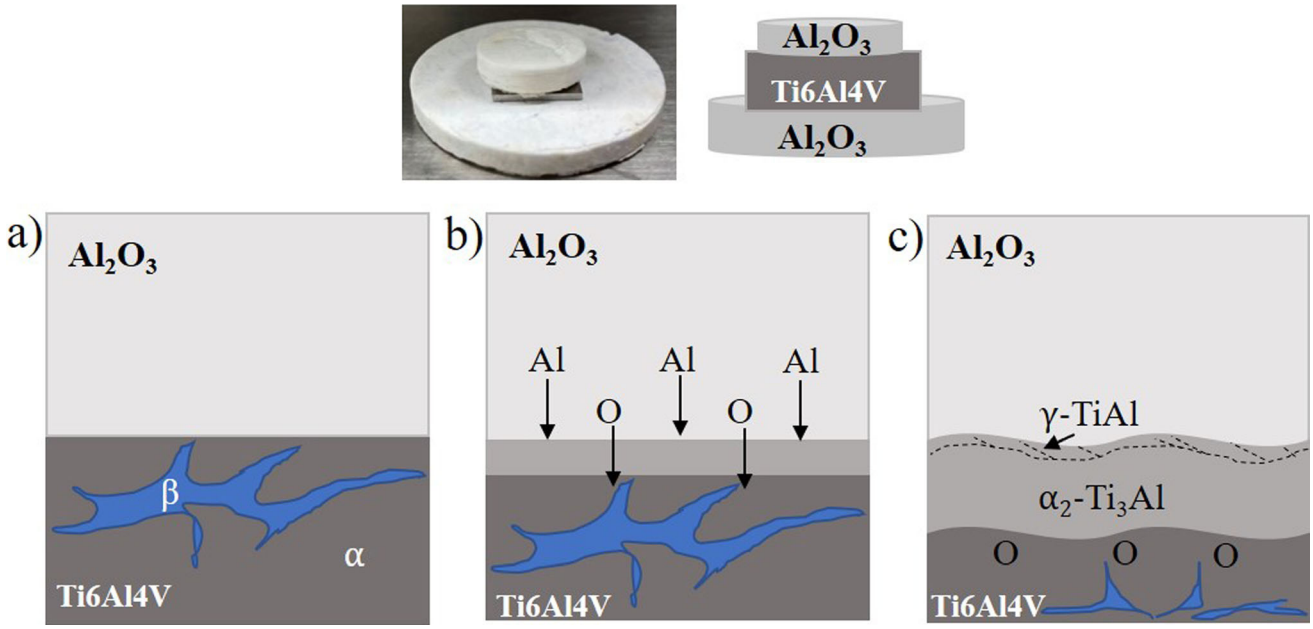

Fig. 11 Illustration of the formation of reaction products on Ti6Al4V in contact with Al_2O_3 during high-temperature processing: (a) Initial microstructure showing the α phase in the matrix and β phase at the grain boundaries, (b) Formation of α-Ti and α_2-Ti_3Al due to diffusion of O_2 and Al, respectively. (c) Growth of the α_2-Ti_3Al layer and formation of a thin γ-TiAl close to Al_2O_3

Such diffusion-driven effects, however, were not observed on the $SrZrO_3$ samples. Explanation of this difference is attributed to the excellent stability of the perovskite structure of $SrZrO_3$. Moreover, while Zr forms a solid solution with Ti as depicted in the Ti-Zr phase diagram (Ref 56), Sr is insoluble in Ti (Ref 57). As a compound, $SrZrO_3$ shows similar insolubility in the Ti-alloy as observed in Fig. 4 and 9. No wonder, additives based on alkaline earth elements like Sr, Ca, Ba, and Mg can be used in the reduction of TiO_x because they are practically insoluble in Ti (Ref 58, 59).

While the methods used in this study were effective for investigating high-temperature interfacial reactions, there are limitations to directly transferring the observations from pellet-based samples to slurry-fabricated molds. Manufacturing shell molds is more complex and involves several steps that impact the ceramic mold structure, properties, and performance. The focus of this work was primarily on refractory material choices to optimize corrosion resistance; as such, future work could explore other properties such as flexural strength, thermal shock resistance, permeability, dimensional stability, and leachability of $SrZrO_3$, which are just as important for investment casting shell molds.

7. Conclusions

This study explored the potential of $SrZrO_3$ as a refractory ceramic for reducing metal-mold reactions with Ti6Al4V compared to Al_2O_3 as used in investment casting. We conducted two types of experiments to understand how Ti6Al4V surfaces are altered when interacting with $SrZrO_3$ and Al_2O_3. The first set of experiments involved diffusion couples of $SrZrO_3$-Ti6Al4V and Al_2O_3-Ti6Al4V, heated and kept for prolonged times below the melting temperature of the titanium alloy. We observed the formation of thick titanium aluminide intermetallics on the surfaces of Ti6Al4V samples in contact with Al_2O_3, while the surface of Ti6Al4V remained clean when coupled with $SrZrO_3$, with no apparent microstructural or surface property variations. The second set of experiments consisted of drop-casting Ti6Al4V onto Al_2O_3 and $SrZrO_3$ in an inert environment. Again, the surface characteristics of Ti6Al4V when cast on Al_2O_3 were drastically different from Ti6Al4V on $SrZrO_3$, with evidence pointing toward aluminum diffusion from Al_2O_3 into the metal, but no perceivable interactions of the titanium alloy with $SrZrO_3$. This work suggests that $SrZrO_3$ could be a promising alternative mold material for investment casting of titanium alloys in high-performance applications, such as aerospace and biomedical industries. Further research is needed to evaluate the performance of $SrZrO_3$ molds made by slurry-based fabrication for commercial-scale manufacturing.

Acknowledgment

We gratefully acknowledge support from the Air Force Research Laboratory, Materials and Manufacturing Directorate (AFRL/RXMS) via Contracts FA8650-18-C-5700 and FA8650-20-C-5206. The sample characterization presented herein were carried out using the equipment in the ThermoFisher Scientific Center for Advanced Microscopy and Materials Analysis (CAMMA), and UConn Tech Park. We also thank Seok-Woo Lee (University of Connecticut) and his group for their help with the nanoindentation experiments.

Conflict of interest

The authors declare that they have no competing financial interests or personal relationships that could have appeared to influence the work reported in this paper.

References

1. I. Gurrappa, Characterization of Titanium Alloy Ti-6Al-4V for Chemical, Marine and Industrial Applications, *Mater. Charact.*, 2003, **51**(2), p 131–139. https://doi.org/10.1016/j.matchar.2003.10.006
2. R.R. Boyer and R.D. Briggs, The Use of β Titanium Alloys in the Aerospace Industry, *J. Mater. Eng. Perform.*, 2005, **14**(6), p 681–685. https://doi.org/10.1361/105994905X75448
3. J.C. Fanning, Military Applications for β Titanium Alloys, *J. Mater. Eng. Perform.*, 2005, **14**(6), p 686–690. https://doi.org/10.1361/105994905X75457
4. M. Geetha, A.K. Singh, R. Asokamani, and A.K. Gogia, Ti Based Biomaterials, the Ultimate Choice for Orthopaedic Implants—A Review, *Prog Mater Sci*, 2009, **54**(3), p 397–425. https://doi.org/10.1016/j.pmatsci.2008.06.004
5. J.T. Philip, J. Mathew, and B. Kuriachen, Tribology of Ti6Al4V: A Review, *Friction*, 2019, **7**(6), p 497–536. https://doi.org/10.1007/s40544-019-0338-7
6. P. Singh, H. Pungotra, and N.S. Kalsi, On the Characteristics of Titanium Alloys for the Aircraft Applications, *Mater. Today Proc.*, 2017, **4**(8), p 8971-8982. https://doi.org/10.1016/j.matpr.2017.07.249
7. C. Cui, B. Hu, L. Zhao, and S. Liu, Titanium Alloy Production Technology, Market Prospects and Industry Development, *Mater. Des.*, 2011, **32**(3), p 1684–1691. https://doi.org/10.1016/j.matdes.2010.09.011
8. R.S. Uwanyuze, J.E. Kanyo, S.F. Myrick, and S. Schafföner, A Review on Alpha Case Formation and Modeling of Mass Transfer During Investment Casting of Titanium Alloys, *J. Alloys Compd.*, 2021, **865**, p 158558. https://doi.org/10.1016/j.jallcom.2020.158558
9. X. Chamorro, N. Herrero-Dorca, P. Rodr'iguez, U. Andr'es, and Z. Azpilgain, Alpha-Case Formation in Ti-6Al-4V Investment Casting Using $ZrSiO_4$ and Al_2O_3 Moulds, *J. Mater. Process. Technol.*, 2017, **243**, p 75–81. https://doi.org/10.1016/j.jmatprotec.2016.12.007
10. G.L. Yu, N. Li, Y.S. Li, and Y.N. Wang, The Effects of Different Types of Investments on the Alpha-Case Layer of Titanium Castings, *J. Prosthet. Dent.*, 2007, **97**(3), p 157–164. https://doi.org/10.1016/j.prosdent.2007.01.005
11. S.-Y. Sung and Y.-J. Kim, Alpha-Case Formation Mechanism on Titanium Investment Castings, *Mater. Sci. Eng. A*, 2005, **405**(1-2), p 173–177. https://doi.org/10.1016/j.msea.2005.05.092
12. R.S. Uwanyuze, S.P. Alpay, S. Schafföner, and S. Sahoo, A First Principles Analysis of Oxidation in Titanium Alloys with Aluminum and Vanadium, *Surf. Sci.*, 2022, **719**, p 122026. https://doi.org/10.1016/j.susc.2022.122026
13. S. Sahoo, S.P. Alpay, and R.J. Hebert, Surface Phase Diagrams of Titanium in Oxygen, Nitrogen and Hydrogen Environments: A First Principles Analysis, *Surf. Sci.*, 2018, **677**, p 18–25. https://doi.org/10.1016/j.susc.2018.05.007
14. S.K. Nayak, C.J. Hung, V. Sharma, S.P. Alpay, A.M. Dongare, W.J. Brindley, and R.J. Hebert, Insight into Point Defects and Impurities in Titanium from First Principles, *NPJ Comput. Mater.*, 2018 https://doi.org/10.1038/s41524-018-0068-9
15. S.-Y. Sung and Y.-J. Kim, Influence of Al Contents on Alpha-Case Formation of Ti-xAl Alloys, *J. Alloys Compd.*, 2006, **415**(1-2), p 93–98. https://doi.org/10.1016/j.jallcom.2005.07.051
16. V. Deshmukh, R. Kadam, and S.S. Joshi, Removal of Alpha Case on Titanium Alloy Surfaces Using Chemical Milling, *Mach. Sci. Technol.*, 2017, **21**(2), p 257–278. https://doi.org/10.1080/10910344.2017.1284558
17. L. Huang, P. Kinnell, and P. Shipway, Parametric Effects on Grit Embedment and Surface Morphology in an Innovative Hybrid Waterjet Cleaning Process for Alpha Case Removal from Titanium Alloys, *Procedia CIRP*, 2013, **6**, p 594–599. https://doi.org/10.1016/j.procir.2013.03.077
18. L. Yue, Z. Wang, and L. Li, Material Morphological Characteristics in Laser Ablation of Alpha Case from Titanium Alloy, *Appl. Surf. Sci.*, 2012, **258**(20), p 8065–8071. https://doi.org/10.1016/j.apsusc.2012.04.173
19. S. Pattnaik, D.B. Karunakar, and P. Jha, Developments in Investment Casting Process: A Review, *J. Mater. Process. Technol.*, 2012, **212**(11), p 2332–2348. https://doi.org/10.1016/j.jmatprotec.2012.06.003
20. L. Nastac, M. Gungor, I. Ucok, K. Klug, and W.T. Tack, Advances in Investment Casting of Ti-6Al-4V: A Review, *Int. J. Cast Met. Res.*, 2006, **19**(2), p 73–93. https://doi.org/10.1179/136404605225023225
21. J.E. Kanyo, S. Schafföner, R.S. Uwanyuze, and K.S. Leary, An Overview of Ceramic Molds for Investment Casting of Nickel Superalloys, *J. Eur. Ceram. Soc.*, 2020, **40**(15), p 4955–4973. https://doi.org/10.1016/j.jeurceramsoc.2020.07.013
22. Y. Cui, X. Tang, M. Gao, L. Ma, and Z. Hu, Interactions Between TiAl Alloy and Different Oxide Moulds under High-Temperature and Long-Time Condition, *High Temp. Mater. Process.*, 2013, **32**(3), p 295–302. https://doi.org/10.1515/htmp-2012-0120
23. J. Kuang, R. Harding, and J. Campbell, Investigation into Refractories as Crucible and Mould Materials for Melting and Casting Gamma-TiAl Alloys, *Mater. Sci. Technol.*, 2000, **16**(9), p 1007–1016. https://doi.org/10.1179/026708300101508964
24. R. Gaddam, M.-L. Antti, and R. Pederson, Influence of Alpha-Case Layer on the Low Cycle Fatigue Properties of Ti-6Al-2Sn-4Zr-2Mo Alloy, *Mater. Sci. Eng. A*, 2014, **599**, p 51–56. https://doi.org/10.1016/j.msea.2014.01.059
25. Z. Abdallah, K. Perkins, and S. Williams, Alpha-Case Kinetics and Surface Crack Growth in the High-Temperature Alloy TIMETAL 834 Under Creep Conditions, *Metall. Mater. Trans. A*, 2012, **43**(12), p 4647–4654. https://doi.org/10.1007/s11661-012-1285-3
26. Y. Venkat, K.R. Choudary, D. Chatterjee, D.K. Das, A.K. Pandey, and S. Singh, Development of Mullite-Alumina Ceramic Shells for Precision Investment Casting of Single-Crystal High-Pressure Turbine Blades, *Ceram. Int.*, 2022, **48**(19), p 28199–28206. https://doi.org/10.1016/j.ceramint.2022.06.124
27. S. Chen, D. Sun, C. Wang, S. Wen, J. Wu, C. Yan, Y. Shi, C. Chen, and Z. Ren, Alumina-Based Ceramic Mold with Integral Core and Shell for Hollow Turbine Blades Fabricated by Laser Powder Bed Fusion, *Addit. Manuf*, 2022, **58**, p 103046. https://doi.org/10.1016/j.addma.2022.103046
28. B.-J. Choi, S. Lee, and Y.-J. Kim, Alpha-Case Reduction Mechanism of Titanium Powder-Added Investment Molds for Titanium Casting, *J. Mater. Eng. Perform.*, 2014, **23**(4), p 1415–1423. https://doi.org/10.1007/s11665-013-0859-6
29. T. Tetsui, T. Kobayashi, T. Ueno, and H. Harada, Consideration of the Influence of Contamination from Oxide Crucibles on TiAl Cast Material, and the Possibility of Achieving low-Purity TiAl Precision Cast Turbine Wheels, *Intermetallics*, 2012, **31**, p 274–281. https://doi.org/10.1016/j.intermet.2012.07.019
30. R.J. Cui, H.R. Zhang, X.X. Tang, L.M. Ma, H. Zhang, and S.K. Gong, Interactions Between Gamma-TiAl Melt and Y_2O_3 Ceramic Material During Directional Solidification Process, *Trans. Nonferr. Met. Soc. China*, 2011, **21**(11), p 2415–2420. https://doi.org/10.1016/S1003-6326(11)61029-7
31. Q. Jia, Y. Cui, and R. Yang, A Study of Two Refractories as Mould Materials for Investment Casting TiAl Based Alloys, *J. Mater. Sci.*, 2006, **41**(10), p 3045–3049. https://doi.org/10.1007/s10853-006-6785-3
32. S.K. Kim, T.K. Kim, M.G. Kim, T.W. Hong, and Y.J. Kim, Investment Casting of Titanium Alloys with CaO Crucible and $CaZrO_3$ Mold, *Lightw. Alloys Aerosp. Appl.*, 2001 https://doi.org/10.1002/9781118787922.ch23
33. D. Eatesami, M.M. Hadavi, and A. Habibollahzade, Melting of γ-TiAl in the Alumina Crucible, *Russ. J. Non-Ferr. Met.*, 2009, **50**(4), p 363–367. https://doi.org/10.3103/S1067821209040105
34. S.K. Sadrnezhad and S.B. Raz, Interaction Between Refractory Crucible Materials and the Melted NiTi Shape-Memory Alloy, *Metall. Mater. Trans. B*, 2005, **36**(3), p 395–403. https://doi.org/10.1007/s11663-005-0068-2
35. U.E. Klotz, C. Legner, F. Bulling, L. Freitag, C. Faßauer, S. Schafföner, and C.G. Aneziris, Investment Casting of Titanium Alloys with Calcium Zirconate Moulds and Crucibles, *Int. J. Adv. Manuf. Technol.*, 2019, **103**, p 1–11. https://doi.org/10.1007/s00170-019-03538-z
36. S. Schafföner, M. Bach, C. Jahn, L. Freitag, and C.G. Aneziris, Advanced Refractories for Titanium Metallurgy Based on Calcium Zirconate with Improved Thermomechanical Properties, *J. Eur. Ceram. Soc.*, 2019, **39**(14), p 4394–4403. https://doi.org/10.1016/j.jeurceramsoc.2019.06.007
37. G. Chen, B. Lan, F. Xiong, P. Gao, H. Zhang, X. Lu, and C. Li, Pilot-Scale Experimental Evaluation of Induction Melting of Ti-46Al-8Nb Alloy in the Fused $BaZrO_3$ Crucible, *Vacuum*, 2019, **159**, p 293–298. https://doi.org/10.1016/j.vacuum.2018.10.050
38. B. Lan, G. Chen, Y. Xiao, Q. Feng, X. Lu, and C. Li, Phase and Microstructural Evolution of $BaZrO_3$-$CaZrO_3$ Refractory and its

Interaction With Titanium Alloy Melt, *Int. J. Appl. Ceram. Technol.*, 2020, **17**(5), p 2193–2201. https://doi.org/10.1111/ijac.13541
39. D.Z. Meng, G.Y. Chen, R.L. Zhang, and C.H. Li, Preparation of Y_2O_3-doped-$SrZrO_3$ Refractory and Study on its Interface Reaction with Molten TiNi Alloys, *Key Eng. Mater.*, 2018, **768**, p 256–260. https://doi.org/10.4028/www.scientific.net/kem.768.256
40. N. S. Jacobson, Thermodynamic properties of some metal oxide-zirconia systems, National Aeronautics and Space Administration, 1989
41. R.A. De Souza, Oxygen Diffusion in $SrTiO_3$ and Related Perovskite Oxides, *Adv. Funct. Mater.*, 2015, **25**(40), p 6326–6342. https://doi.org/10.1002/adfm.201500827
42. W. Ma, D.E. Mack, R. Vaßen, and D. Stöver, Perovskite-Type Strontium Zirconate as a New Material for Thermal Barrier Coatings, *J. Am. Ceram. Soc.*, 2008, **91**(8), p 2630–2635. https://doi.org/10.1111/j.1551-2916.2008.02472.x
43. M. Zborowska, M. Grylicki, and J. Zborowski, The Preparation and Properties of Strontium Zirconate Ceramics for Channels of Open-Cycle MHD Generators, *Ceramurg. Int.*, 1980, **6**(3), p 99–102. https://doi.org/10.1016/0390-5519(80)90020-4
44. A.B. Tuğrul, H.Ö. Toplan, B. Büyük, E. Demir, G. Sönmez, S. Kurt, and N. Toplan, Plasma-Sprayed Strontium Zirconate Coatings, *Appl. Phys. A*, 2021, **127**(8), p 592. https://doi.org/10.1007/s00339-021-04736-x
45. A. Pragatheeswaran, P.V. Ananthapadmanabhan, Y. Chakravarthy, S. Bhandari, T.K. Thiyagarajan, N. Tiwari, T.K. Saha, and K. Ramachandran, Plasma Spray Deposition and Characterization of Strontium Zirconate Coatings, *Ceram. Int.*, 2014, **40**(7), p 10441–10446. https://doi.org/10.1016/j.ceramint.2014.02.128
46. P. Kaur and K. Singh, Structural, Thermal and Electrical Study of Copper-Doped Strontium Zirconate, *Ionics*, 2020, **26**(12), p 6233–6244. https://doi.org/10.1007/s11581-020-03752-w
47. J.E. Kanyo, R.S. Uwanyuze, J. Zhang, R.J. Hebert, S. Schafföner, and L. Frame, Solid-State Calcination and Synthesis of Homogeneous Strontium Zirconate by Slip Casting", *Solid State Sci.*, 2023, **142**, p 107235. https://doi.org/10.1016/j.solidstatesciences.2023.107235
48. S. Lee and Y.-J. Kim, Evaluation of the Alpha-Case with TiO_2 in Mold for Titanium Investment Casting, *Int. J. Met.*, 2017, **11**(1), p 71–76. https://doi.org/10.1007/s40962-016-0093-8
49. M. J. Donachie, *Titanium: A Technical Guide, 2nd Edition*. ASM International, 2000
50. F.H. Hayes, The Al-Ti-V (Aluminum-Titanium-Vanadium) System, *J. Phase Equilibria*, 1995, **16**(2), p 163–176. https://doi.org/10.1007/BF02664854
51. S.L. Semiatin, T.M. Brown, T.A. Goff, P.N. Fagin, R.E. Turner, J.M. Murry, D.R. Barker, J.D. Miller, and F. Zhang, Diffusion Coefficients for Modeling the Heat Treatment of Ti-6Al-4V, *Metall. Mater. Trans. A*, 2004, **35**(9), p 3015–3018. https://doi.org/10.1007/s11661-004-0250-1
52. V. Maurice, G. Despert, S. Zanna, P. Josso, M.-P. Bacos, and P. Marcus, XPS Study of the Initial Stages of Oxidation of α_2-Ti_3Al and γ-TiAl Intermetallic Alloys, *Acta Mater.*, 2007, **55**(10), p 3315–3325. https://doi.org/10.1016/j.actamat.2007.01.030
53. B.-J. Lee, and N. Saunders, Thermodynamic Evaluation of the Ti-Al-O Ternary System, *Int. J. Mater. Res.*, 1997, **88**(2), p 152–161. https://doi.org/10.3139/ijmr-1997-0028
54. M. Silva, A.S. Ramos, and S. Simões, Joining Ti6Al4V to Alumina by Diffusion Bonding Using Titanium Interlayers, *Metals*, 2021, **11**(11), p 1728. https://doi.org/10.3390/met11111728
55. A.M. Kliauga and M. Ferrante, Interface Compounds Formed During the diffusion Bonding of Al_2O_3 to Ti, *J. Mater. Sci.*, 2000, **35**(17), p 4243-4249. https://doi.org/10.1023/A:1004815830980
56. J.L. Murray, The Ti−Zr (Titanium-Zirconium) System, *Bull. Alloy Phase Diagr.*, 1981, **2**(2), p 197–201. https://doi.org/10.1007/BF02881478
57. A.A. Yaremchenko, S.G. Patrício, and J.R. Frade, Thermochemical Behavior and Transport Properties of Pr-Substituted $SrTiO_3$ as Potential Solid Oxide Fuel Cell Anode, *J. Power Sources*, 2014, **245**, p 557–569. https://doi.org/10.1016/j.jpowsour.2013.07.019
58. R.O. Suzuki, Direct Reduction Processes for Titanium Oxide in Molten Salt, *JOM*, 2007, **59**(1), p 68–71. https://doi.org/10.1007/s11837-007-0014-7
59. M. Ye, J. Jia, Z. Wu, C. Qian, R. Chen, P.G. O'Brien, W. Sun, Y. Dong, and G.A. Ozin, Synthesis of BLACK TiOx Nanoparticles by Mg Reduction of TiO_2 Nanocrystals and their Application for Solar Water Evaporation, *Adv. Energy Mater.*, 2017, **7**(4), p 1601811. https://doi.org/10.1002/aenm.201601811